Polymer Bulletin (2022) 79:9697–9716
https://doi.org/10.1007/s00289-021-03973-7

ORIGINAL PAPER

Amino acid-metal phosphate hybrid nanoflowers (AaHNFs): their preparation, characterization and anti-oxidant capacities

N. Özdemir[1] · C. Altinkaynak[2] · M. Türk[1] · F. Geçili[1] · S. Tavlaşoğlu[1]

Received: 17 April 2021 / Revised: 16 November 2021 / Accepted: 16 November 2021 /
Published online: 25 November 2021

Abstract

Reactive oxygen species like hydrogen peroxide have positive roles in vivo systems such as phagocytosis, intercellular signal transfer, regulation of cell growth, and the synthesis of important biological compounds. Nanostructures can exhibit increased redox and radical scavenging activities compared to the free form with peroxidase-like activities. This work presents the synthesis and characterization of amino acid-metal phosphate hybrid nanoflowers (AaHNFs) and their potential as a radical scavenger and anti-oxidant. The AaHNFs were synthesized using some metal ions (Cu^{2+}, Mn^{2+}, Ni^{2+}, Co^{2+}, and Zn^{2+}) and selected amino acids (His, Cys, Asn, and Asp) which contain an imidazole ring, sulfhydryl, carboxamide, and carboxylate groups. Synthesized AaHNFs were characterized by their morphology and chemical point of view by using different techniques such as SEM, EDX, FTIR and XRD. Their peroxidase like activities were determined. Using the principle of Fenton's reaction, AaHNFs were found to be exhibitinga more effective peroxidase-like activity than free amino acids. We applied different analytical measurement methods such as hydrogen peroxide scavenging activity assay of AaHNFs and the assays of DPPH and ABTS radical scavenging activities to determine the anti-oxidant capacities of AaHNFs. AaHNFs can be evaluated as an effective anti-oxidant scavenger material due to their superior properties. This new type of HNFs can be exploited as a natural anti-oxidant in various potential applications related to fields such as biosensing, bioassay, biomedicine, pharmaceutics and biocatalysis.

✉ N. Özdemir
ozdemirn@erciyes.edu.tr

[1] Faculty of Science, Chemistry Department, Biochemistry Division, Erciyes University, 38039 Kayseri, Turkey

[2] Department of Plant and Animal Production, Avanos Vocational School, Nevşehir Haci Bektas Veli University, 50500 Nevşehir, Turkey

Keywords Amino acids · Hybrid nanoflowers · Metal ions · Peroxidase-like activity · Anti-oxidant capacity

Introduction

Superoxide anion (O^{2-}), hydrogen peroxide (H_2O_2), and hydroxyl radicals (·OH) are reactive oxygen species that include very toxic components [1]. The presence of excessive reactive oxygen species (ROS) generated as byproducts of aerobic metabolism leads to mutations and cell death by damaging proteins, lipids, and DNA in the human body [2]. In biological systems, there are defense mechanisms called simply antioxidants to prevent the damages such as aging, cancer, cardiovascular diseases, and Alzheimer's caused by ROS and free radicals. Although natural antioxidants are widely used to prevent these damages, their use there is inhibited by factors including low solubility, sensitivity to light, low levels of oxygen and pH, poor target specificity, poor bioavailability, and high side effects when used at high levels [3–5]. In the last decade, to overcome these limitations, new materials such as nanostructures and hybrid materials which were synthesized through new technology and methods started to be used instead of traditional antioxidants. Organic–inorganic hybrid nanoflowers exhibit improved bioactivity and antioxidant activity compared to their free form due to their ability to encapsulate high amounts of organic molecules in the structure.

Organic–inorganic hybrid nanoflowers as an important biomolecule immobilization method were first reported by Zare and co-workers [6]. The hybrid nanoflowers have gained tremendous attention from researchers [7, 8]. Until now, different kinds of hybrid nanoflowers have been synthesized for several applications such as biosensors [9], dye decolorization [10], catalysis [11], biological analysis [12], and pharmaceuticals [13]. In addition, various biomolecules such as protein [14], enzyme [15], DNA [16–18], antibody [19], plant extracts [20, 21], and amino acids [22] have been utilized as organic components for the synthesis of hybrid nanoflowers. When proteins or enzymes are used as the organic component, the hybrid nanoflowers show increased activities compared to free molecules [10]. The synthesis conditions, particularly the type and amount of both organic and inorganic components, affect the composition and morphology of the hybrid materials and ultimately the functions of hybrid materials [23].

As it is known, proteins are biopolymers of amino acids (Aa) [24–26]. Amino acids can be divided into three main groups: acidic, basic, and neutral [24]. Their characteristics vary according to their groups. Shi and co-workers reported that L-Glu and L-Asp exhibited an intrinsic peroxidase-like activity against the TMB substrate [24]. They used these amino acids to detect H_2O_2 and glucose and to measure the anti-oxidant behaviors. They particularly investigated the side-chain effect on the peroxidase-like activity and reported that when the side-chain had -COOH, peroxidase-like activity was seen [24], and if the side-chain was replaced with -H, -OH, -SH or $CONH_2$, mimic activity could hardly be seen. Singh and co-workers developed asparagine functionalized magnetic nanoparticles to apply for Ni (II) adsorption [27]. Chandra and Singh reported a green approach to the

biosynthesis of amino acid-functionalized silver nanoparticles using neem gum which can be promising for a natural mechanism of oxygen sensing [26]. In addition, Sun and co-workers reported that the C=O groups were the catalytically active sites, whereas the O=CO groups acted as substrate-binding sites, and COH groups could inhibit the peroxidase-like activity [28].

Amino acids are strongly bound to some transition metal ions (especially Cu^{2+}) to generate complexes, and their types of side chains play an important role in the complex formation [25, 29–31]. Under certain conditions, the interaction between amino acids and metal ions allows the formation of hybrid structures with flower-like shapes. Amino acids incorporated hybrid nanoflowers were firstly reported by Wu and co-workers. Twenty standard amino acids as the organic component and Cu^{2+} ion as the inorganic component were used by the researchers for the synthesis of the hybrid nanoflowers [22]. They investigated the peroxidase-like activity of the synthesized hybrid structures against ABTS and Rhodamine B as substrates and suggested that peroxidase-like activity follows a Fenton-like reaction mechanism. Several related studies claiming that this mechanism is followed in organic–inorganic hybrid nanoflowers have also been reported [32–34]. In one study regarding the peroxidase activity of amino acids, it was shown that the type of side chains of amino acids directly affect the peroxidase-like activity of free amino acids [35], while in another study side chains in the hybrid structure caused a change in this type of activity as follows: positively charged R groups > nonpolar, aliphatic R groups > aromatic R groups > polar, uncharged R groups > negatively charged R groups [22].

As mentioned before, for the synthesis of organic–inorganic hybrid nanoflowers, various types of organic molecules were used as the organic component and some divalent metal ions (Ni^{2+}, Ca^{2+}, Mn^{2+}, Co^{2+}, and Zn^{2+}, etc.) particularly Cu^{2+} ion as the inorganic component [36, 37, 39, 40].

To the best of our knowledge, no investigation was reported on the synthesis of amino acid incorporated hybrid nanoflowers using divalent metal ions (Mn^{2+}, Ni^{2+}, Co^{2+}, and Zn^{2+}) except Cu^{2+}. In this study, we synthesized amino acid-metal phosphate hybrid nanoflowers (AaHNFs) using some metal ions (Cu^{2+}, Mn^{2+}, Ni^{2+}, Co^{2+}, and Zn^{2+}) and selected amino acids (His, Cys, Asn, and Asp) which contain an imidazole ring, sulfhydryl, carboxamide and carboxylate groups. Unlike the previous study reported by Wu et al., we used four novel metal ions (Mn^{2+}, Ni^{2+}, Co^{2+}, and Zn^{2+}) besides the Cu^{2+} in our study to synthesize AaHNFs for the first time. Wu and co-workers reported in their study that the synthesized amino acid-Cu^{2+} HNFs showed enhanced peroxidase-like activity and these activities proceed through the Fenton mechanism [22]. Fenton reagents act as radical scavengers [38]. This study also aims to investigate the anti-oxidant capacity of AaHNFs. For this purpose, we applied different analytical measurement methods such as hydrogen peroxide scavenging activity assay of AaHNFs, and the assays of DPPH and ABTS radical scavenging activities for detecting the anti-oxidant capacity of AaHNFs.

Experimental

Materials

L-Cysteine hydrochloride monohydrate, ascorbic acid, copper sulfate pentahydrate ($CuSO_4{\cdot}5H_2O$), cobalt (II) sulfate heptahydrate ($CoSO_4{\cdot}7H_2O$), zinc acetate dihydrate ($Zn(CH_3COO)_2{\cdot}2H_2O$), sodium dihydrogen phosphate (NaH_2PO_4), calcium chloride dihydrate ($CaCl_2{\cdot}2H_2O$), magnesium chloride ($MgCl_2$), potassium chloride (KCl), sodium hydroxide (NaOH), 2,2-diphenyl-1-(2,4,6-trinitrophenyl) hydrazyl (DPPH), 2,2′-azino-bis(3-ethylbenzothiazoline-6-sulfonic acid) diammonium salt (ABTS), potassium persulfate ($K_2S_2O_8$), ethanol, hydrochloric acid (HCl) and guaiacol were purchased from Sigma-Aldrich (USA) and zinc acetate dihydrate ($Zn(CH_3COO)_2{\cdot}2H_2O$) from Carlo Erba. Nickel (II) sulfate hexahydrate ($NiSO4{\cdot}6H_2O$), manganese sulfate monohydrate ($MnSO_4{\cdot}H_2O$), sodium chloride (NaCl), potassium phosphate dibasic (KH_2PO_4), disodium hydrogen phosphate (Na_2HPO_4), and hydrogen peroxide (H_2O_2) were obtained from Merck. All the reagents used for the experiments were of analytical grade. The substrate solutions used for each experiment were freshly prepared in sufficient amounts.

Preparation of AaHNFs

The preparation procedure of the AaHNFs was carried out as described previously [15, 16]. For Aa-Cu^{2+}, Aa-Mn^{2+}, and Aa-Ni^{2+} HNFs; a 120 mM metal ion solution was prepared. A certain amount of metal ion stock solution was mixed with the 10 mM PBS at different pH levels (pH 5–9) containing 0.02 mg/mL amino acids. Then, the mixtures were vortexed vigorously and incubated without disturbing at RT for 3 days. At the end of the incubation period, the precipitates were centrifuged at 5000 rpm for 10 min to remove unbounded molecules. Finally, the synthesized AaHNFs were washed with pure water at least 3 times and dried at 30 °C.

Aa-Co^{2+} and Aa-Zn^{2+} HNFs were synthesized following the previous works with slight modifications [4, 22, 34]. 1.6 mL of Cobalt (II) sulfate heptahydrate solution (0.05 g/mL) and zinc acetate (0.05 g/mL) were added separately into 20 mL of PBS (10 mM) at different pH levels containing 16 mg amino acid. Each mixture was stirred on a magnetic stirrer at RT for 3 h and 3 days, respectively. At the end of the incubation period, the solutions were centrifuged at 5000 rpm for 10 min to remove unbounded molecules. The synthesized AaHNFs were washed with pure water at least 3 times and dried at 30 °C.

Characterization of AaHNFs

Some devices and techniques were used to characterize the synthesized AaHNFs. The SEM images and EDX analyses of AaHNFs were obtained by using SEM (Leo 440 computer controlled digitally, Leica, Jena, Germany). FTIR analyses were conducted on a FTIR spectrometer (PerkinElmer 400, USA). Bruker X-ray diffraction

spectroscopy (Bruker AXS D8 Advance Model, Germany) was used for the XRD analyses of AaHNFs.

Evaluation of peroxidase mimic activity of AaHNFs

The method is based on measuring by catalyzing the dehydrogenation of guaiacol as substrate [40]. In peroxidase mimic activity assays of AaHNFs, first, 1 mL of 45 mM guaiacol, 1 mL of 22.5 mM H_2O_2, and 1 mL of PBS buffer at different pH levels (pH 5–9) were mixed separately. Then, 3 mg of AaHNFs was added into the experiment tubes to start the reaction. Next, the reaction tubes were incubated for 25 min at RT. After that, at the end of the incubation period, the mixture was centrifuged at 5000 rpm for 5 min. Finally, the supernatants were separated and read at 470 nm. The experiment was repeated three times.

Hydrogen peroxide scavenging activity of AaHNFs

The hydrogen peroxide scavenging ability of the AaHNFs was studied with the method described by Ruch et al. [41]. In the first step, 43 mM H_2O_2 stock solution was prepared in 0.1 M of phosphate buffer (pH 7.4) which contained 0.2 M KH_2PO_4 and 0.1 M NaOH. After the AaHNFs were dispersed in a 3.4 mL of phosphate buffer solution, 0.6 mL of 43 mM H_2O_2 stock solution was also added. These mixtures were incubated for 10 min and then centrifuged at 5000 rpm for 3 min. The absorbance values of supernatants were recorded at 230 nm. Hydrogen peroxide scavenging activity was calculated by the equation of % H_2O_2 scavenging activity = $\{1\text{-}(Abs_{Sample}/Abs_{Control}\} \times 100$, where $Abs_{Control}$ was the absorbance of reaction solution without sample and the blank solution was phosphate buffer. The experiment was repeated three times at each concentration.

DPPH radical scavenging activity of AaHNFs

DPPH free radical scavenging ability of the AaHNFs was determined using the method proposed by Blois [42] with some modifications. First, sample solutions at different concentrations (1000 ppm-50 ppm) were prepared by adding AaHNFs in 1.5 mL ethanol. Then, 0.5 mL of 0.1 mM DPPH (in ethanol) was added to the 1.5 mL sample solution. Next, the reaction solution was vortexed and incubated in a dark place for 30 min. After the incubation period, the reaction solution was centrifuged at 5000 rpm. After that, the absorbance of the supernatant was recorded spectrophotometrically at 517 nm. DPPH free radical scavenging ability was calculated by using the equation of % DPPH radical scavenging activity = $\{1\text{-}(Abs_{Sample}/Abs_{Control})\} \times 100$, where $Abs_{Control}$ was the absorbance of reaction solution without sample and the blank solution was ethanol. Finally, the experiment was repeated three times at each concentration.

ABTS radical scavenging activity of AaHNFs

ABTS free radical scavenging ability of the AaHNFs was carried out by the method proposed by Re et al. [43]. Firstly, ABTS radical was obtained by mixing 2 mM of ABTS (in ethanol) and 2.45 mM of $K_2S_2O_8$ and this solution was incubated in a dark place for 4 h. Then, the ABTS radical solution was diluted to form a 0.75 Abs at 734 nm by using 0.1 M Na phosphate buffer (pH 7.4). Next, 1 mL of ABTS radical solution and 3 mL of sample solution (in H_2O) were mixed and incubated for 30 min. After the incubation period, the solution was centrifuged at 5000 rpm. After that, the supernatant was measured spectrophotometrically at 734 nm. ABTS radical scavenging activity of AaNHFs was calculated using the formula of % $ABTS^+$ radical scavenging activity = $[1\text{-}(Abs_{Sample}/Abs_{Control}] \times 100$, where $Abs_{Control}$ was the absorbance of reaction solution without sample and the blank solution was H_2O. Finally, the experiment was repeated three times at each concentration.

Results and discussion

Preparation and characterization of AaHNFs

It's well known that certain biomolecules such as proteins and enzymes can easily coordinate and make complexes with some metal ions [44] because of their strong affinity thanks to the amide groups in their backbones. Amino acids can also make complexes with the metal ions and under certain conditions, the interaction between the amino acids and some metal ions can allow the formation of hybrid structures with flower-like shapes. The organic–inorganic HNFs are prepared simply by mixing organic and inorganic components. In the synthesis procedure, the types and concentrations of both organic and inorganic components affect the composition, morphology, and ultimately function of HNFs. Several comprehensive studies were performed to shed light on the formation mechanism of organic–inorganic HNFs [7, 13, 15, 45].

The formation mechanism of AaHNFs is shown in Fig. 1. Firstly, primary metal phosphate nanocrystals are formed in the nucleation step. Then, these primary metal phosphate nanocrystals interact simultaneously with the amino acids. These interactions between metal ions of the primary metal phosphate nanocrystals and N atoms of the amino acids form leaf-like amino acid metal phosphate nanoplates. Finally, the multi-layered flower-like structures are obtained as a result of the anisotropic growth of the nanoplates.

Until now, there is only one study about amino acid incorporated HNFs reported by Wu et al. They reported that the synthesized amino acid-Cu^{2+} HNFs showed enhanced peroxidase-like activity [22]. To the best of our knowledge, there is no information about the formation of amino acid-metal phosphate hybrid nanoflowers (AaHNFs) using different metal ions except copper. Therefore, in our study, we synthesized AaHNFs by using four more metal ions called Mn^{2+}, Ni^{2+}, Co^{2+}, Zn^{2+} besides Cu^{2+} and selected amino acids (His, Cys, Asn, and Asp) which contain imidazole ring, sulfhydryl, carboxamide, and carboxylate groups. As mentioned before,

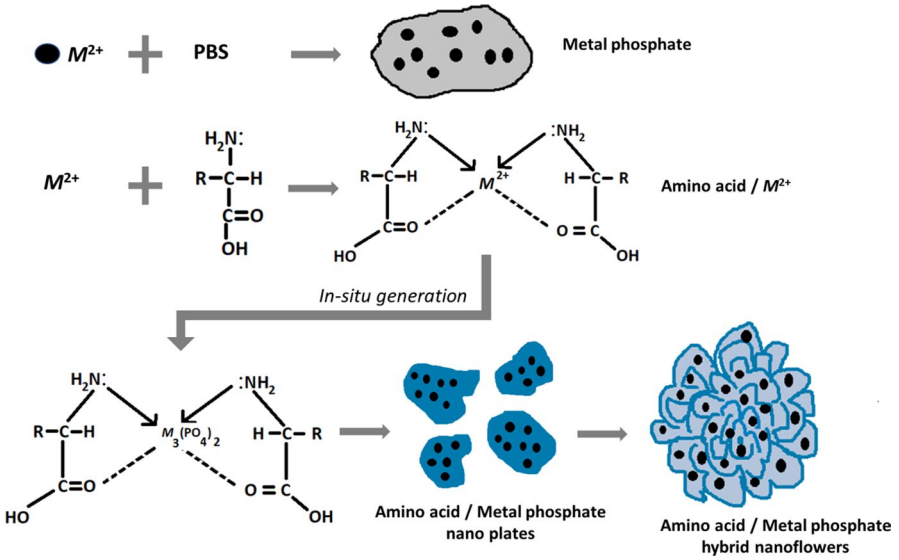

Fig. 1 The formation mechanism of AaHNFs

types and concentrations of organic and also inorganic components affect the formation of flower-like morphology and function of HNFs. For this reason, AaHNFs were synthesized in the pH range from 5 to 9 by using some amino acids and metal ions as described in the experimental procedure section above. The product formation results of AaHNFs were presented in Table S1. As shown in Table S1, for all amino acids and metal ions used in the synthesis, no product was obtained at pH 5 because of the strong repulsion between amino acids and metal ions. SEM images of Aa-Cu^{2+} HNFs synthesized at pH 7 are given in Fig. 2.

Asn-Cu^{2+}, Asp-Cu^{2+}, and His-Cu^{2+} HNFs had a ball-shaped and uniformly distributed morphology, while Cys-Cu^{2+} hybrid nanoflowers had a slightly different shape and morphology (Fig. 2). It is well known that the changes in surface morphology and area affect the biological activity of the hybrid material [23]. Wu and co-workers synthesized the amino acids incorporated HNFs at only one pH level (pH 7.4) [22]. Unlike their study, both the effect of pH on the morphologies of AaHNFs and the formation of Aa-Cu^{2+} HNFs at different pH values were evaluated in our study. SEM images of Aa-Cu^{2+} HNFs synthesized at different pH levels are given in Fig S1-S4.

SEM images of Aa-Co^{2+} HNFs synthesized under optimum conditions are given in Fig. 3.

As seen in Fig. 3, when we use Co^{2+} as the inorganic part, the hybrid morphology looked slightly different from the structure obtained with Cu^{2+}. The optimum synthesis pH levels of Asn-Co^{2+}, Asp-Co^{2+}, Cys-Co^{2+}, and His-Co^{2+} HNFs were determined to be pH 7, pH 8, pH 7, and pH 6, respectively (Fig. 2). While Asn-Co^{2+} and Asp-Co^{2+} HNFs were shaped rose flower-like, the plates of Asn-Co^{2+} HNFs were thinner than Asp-Co^{2+} HNFs. The morphology of His-Co^{2+} HNFs

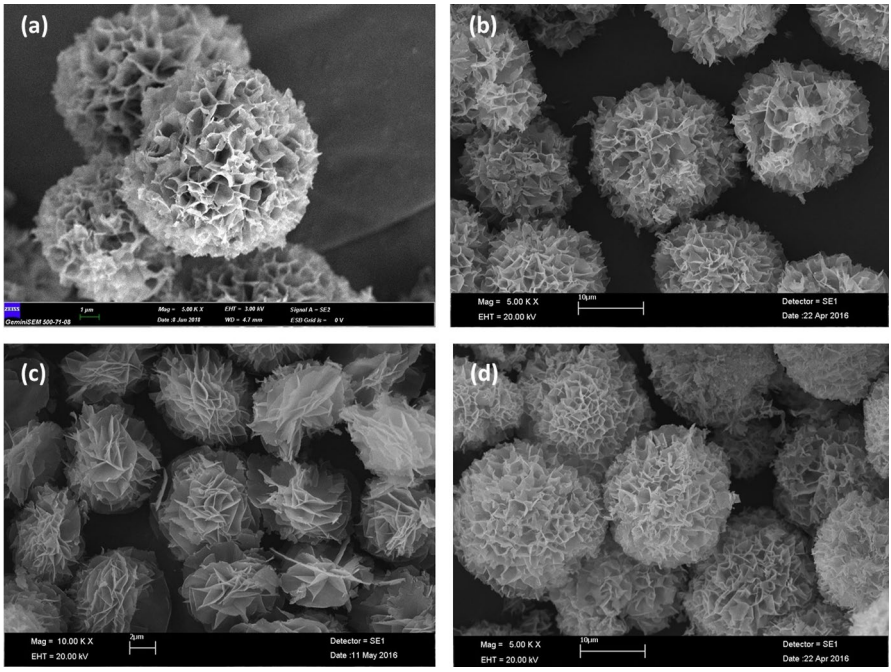

Fig. 2 SEM images of Aa-Cu^{2+} HNFs; **a** Asn-Cu^{2+}, **b** Asp-Cu^{2+}, **c** Cys-Cu^{2+}, and **d** His-Cu^{2+} hybrid nanoflowers

was similar to that of the Cu^{2+} synthesized one. Unlike these, the leaves of Cys-Co^{2+} HNFs were thicker than the leaves of the other three and anchored at the center of the nanoflower. There was no product obtained at pH 5 and pH 6 for Asp-Co^{2+} HNFs (Table S1). SEM images of Aa-Co^{2+} HNFs obtained at different pH levels are shown in Figures S5–S8.

When Mn^{2+} ion was used, no product formation was observed at pH 5 and pH 6 (Table S1). At higher pH values, although product formation was observed, no Aa-Mn^{2+} HNFs formation could be observed. SEM images of Aa-Mn^{2+} hybrid structures are shown in Figures S9–S12.

When the Zn^{2+} ion was used as the inorganic part, the obtained morphologies were generally similar to the rose shape. The optimum pH levels of Asn-Zn^{2+}, Asp-Zn^{2+}, Cys-Zn^{2+}, and His-Zn^{2+} HNFs were determined to be pH 6, pH 8, pH 7, and pH 7, respectively (Fig. 4). Cys-Zn^{2+} HNFs had plates thicker than those in the other three nanostructures (Fig. 4c).

When Ni^{2+} ion was used as the inorganic part, no product was observed at different pH levels (Table S1). After determining the optimum synthesis pHs of AaHNFs, EDX analysis was performed to confirm the presence of the respective metal ions, C, P, N, and O (Figure S17).

XRD analysis in Figures S18–S20 proved the crystal structures of the nanoflowers and metal-phosphates. All diffraction peaks of metal-phosphates matched well

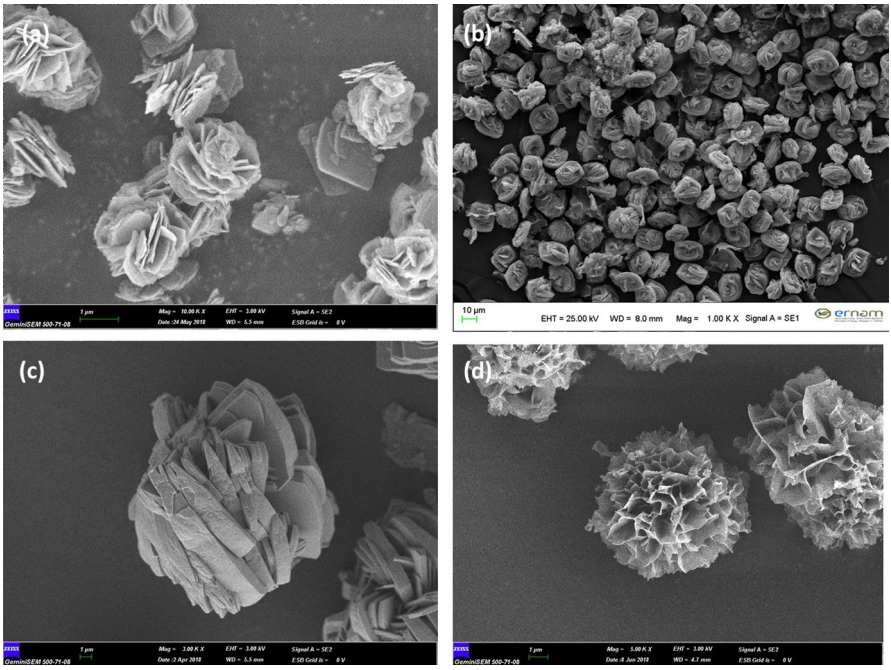

Fig. 3 SEM images of Aa-Co^{2+} HNFs; **a** Asn-Co^{2+}, **b** Asp-Co^{2+}, **c** Cys-Co^{2+}, and **d** His-Co^{2+} HNFs

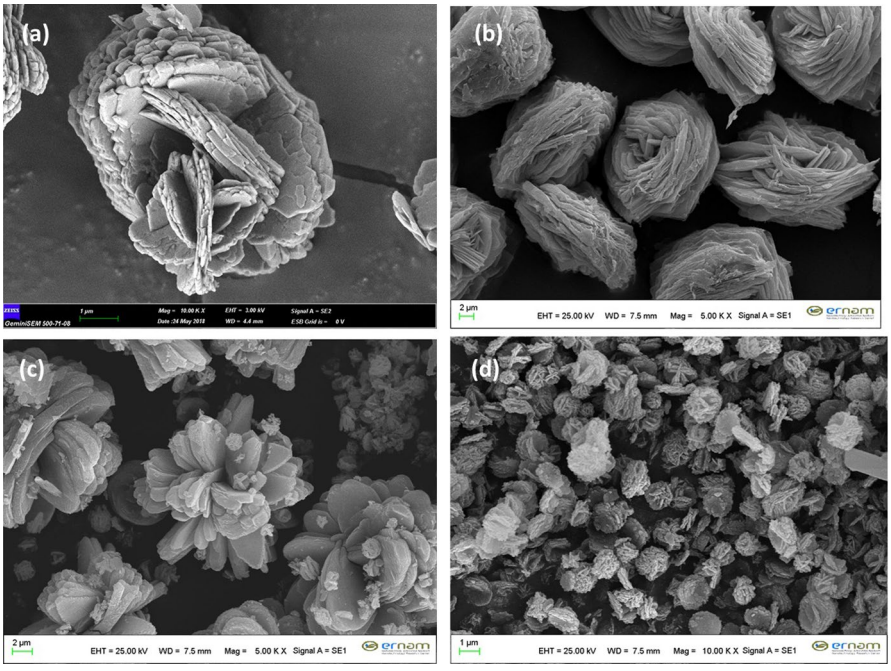

Fig. 4 SEM images of Aa-Zn^{2+} HNFs; **a** Asn-Zn^{2+}, **b** Asp-Zn^{2+}, **c** Cys-Zn^{2+}, and **d** His-Zn^{2+} HNFs

with those obtained from the JCPDS cards. The formed crystals of metal phosphate provided the major skeleton of the nanoflower.

The results of the FTIR analysis of AaHNFs and free amino acids are presented in Figures S21–S24. The characteristic absorbance bands of amino acids can be observed clearly in the nanoflowers.

Evaluation of peroxidase mimic activities of AaHNFs

The peroxidase mimic activities of AaHNFs were examined with the peroxidase substrate, Guaiacol, in the presence of H_2O_2. The AaHNFs were obtained in the optimum conditions. The AaHNFs can act as a Fenton-like reaction [9, 33]. The parameters at different pH values were scanned to determine the optimum peroxidase mimic activity of AaHNFs. The peroxidase mimic activity results of the AaHNFs obtained by using copper ion are given in Fig. 5. According to this result, His-Cu^{2+} hybrid nanoflowers showed the highest peroxidase activity value at pH 8. This value was followed by Asn-Cu^{2+} hybrid nanoflowers at pH 8 as 84.4%. The highest peroxidase activities for Cys-Cu^{2+} and Asp-Cu^{2+} hybrid nanoflowers were determined at pH 7. Asp-Cu^{2+} and Cys-Cu^{2+} hybrid nanoflowers exhibited 67.5% and 52.9% higher activity than phosphate crystals and other hybrid nanoflowers, respectively. Shi and co-workers found that free amino acids such as L-Glu and L-Asp displayed peroxidase mimic activity like HRP [24]. They used the peroxidase mimic properties of these amino acids in a colorimetric glucose test system to determine in the range of 0.1–10 μM. In the first work related to amino acid-incorporated nanoflowers, Wu and co-workers employed all amino acids with copper ions to prepare hybrid nanoflowers for peroxidase mimics [22]. Using ABTS as substrate, they found that peroxidase mimic activities of Asp nanoflower, Asparagine nanoflower, Cysteine nanoflower, and Histidine nanoflower were 0.00799, 0.00889, 0.00901, and 0.01347 μmol/mg/min, respectively. As we know, these amino acids have different side chains. Histidine has an imidazole ring, cysteine has a sulfhydryl group, asparagine has a carboxamide group, and finally, aspartate has an acidic side chain (CH_2COOH). As shown in Fig. 5, when the peroxidase mimics of amino acid-metal phosphate hybrid nanoflowers are compared, it is seen that those activities were in

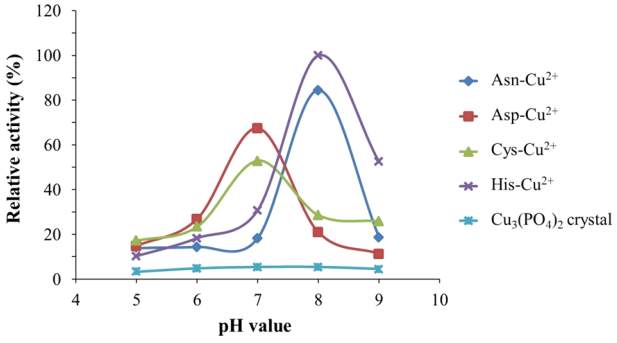

Fig. 5 Enzymatic activity values of AaHNFs and $Cu_3(PO_4)_2$ crystal in different pH conditions

a decreasing manner as follows: His > Asn > Asp > Cys. When they are evaluated according to the type of amino acid side groups, peroxidase mimic activities were in a manner changing from + charged to -charged as follows: positively charged R group > polar > negatively charged groups. We confirmed the similar results reported in the article by Wu and co-workers [22]. The positively charged R groups of amino acids created more hydroxyl radicals and increased their peroxidase mimic level. Additionally, we examined how the other AaHNFs influenced the peroxidase mimics on the same chart. We just separated the metal types for a clearer understanding of the data.

The highest peroxidase activities for Asn-Co^{2+}, Asp-Co^{2+}, Cys-Co^{2+}, and His-Co^{2+} HNFs were determined to be at pH 6, pH 7, pH 8, and pH 5, respectively (Fig. 6). The peroxidase mimics of amino acid-Co^{2+} phosphate HNFs were determined to be 59.16%, 53.63%, 48.78%, and 49.82% for Asn-Co^{2+} HNFs, Asp-Co^{2+} HNFs, Cys-Co^{2+} HNFs, and His-Co^{2+} HNFs, respectively. The highest peroxidase activities for His-Zn^{2+}, Asp-Zn^{2+}, Cys-Zn^{2+}, and Asn-Zn^{2+} HNFs were determined to be at pH 7, pH 7, pH 9, and pH 5, respectively (Fig. 7). For amino acid-Zn^{2+} phosphate HNFs, the values of peroxidase mimics were determined to be 35.29% for His-Zn^{2+} HNFs, 30% for Asp-Zn^{2+} HNFs, 29.75% for Cys-Zn^{2+} HNFs, and 27.33% for Asn-Zn^{2+} HNFs. Interestingly, the peroxidase mimic activity of His-Cu^{2+} and His-Zn^{2+} HNFs was higher within their group, but they showed the lowest activity among the structures obtained with Co^{2+} metal. To compare the activities of metal crystals with AaHNFs, the activities of metal phosphate crystals were very low.

Hydrogen peroxide scavenging activity of AaHNFs

Although hydrogen peroxide is not a free radical, it is very important due to its oxidizing properties. H_2O_2 inactivates several cell enzymes by penetration to the biological membranes in the human body. Inactivated enzymes can bring on cell damage. Due to its oxidizing property, H_2O_2 plays a mediator role in the production of ROS species through Fenton (1) and Haber- Weiss (2) reactions [46]. Decomposition

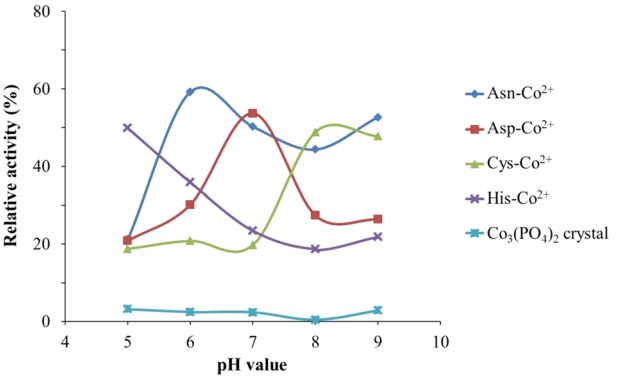

Fig. 6 Enzymatic activity values of AaHNFs and $Co_3(PO_4)_2$ crystal in different pH conditions

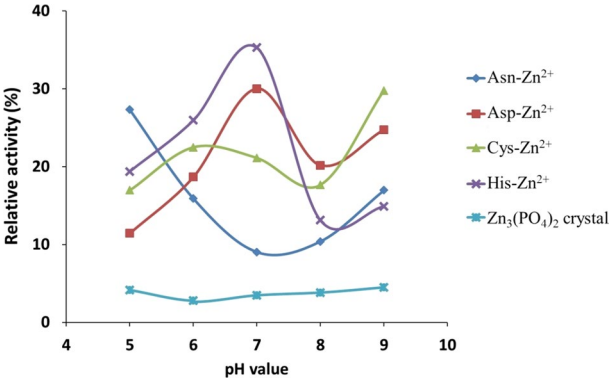

Fig. 7 Enzymatic activity values of AaHNFs and $Zn_3(PO_4)_2$ crystal at different pHs

of H_2O_2 causes a decrease in the level of oxidative stress in vivo depending on the reduction in ROS level.

$$Fe^{2+} + H_2O_2 - - - - - - - - Fe^{3+} + OH^- + OH^{\cdot} \quad (1)$$

$$O_2^{-} + H_2O_2 - - - - - - - - - - - - O_2 + OH^- + OH \quad (2)$$

As shown in Table 1, we compared the Aa-metal phosphate hybrid nanoflower's H_2O_2 scavenging activities of the metal phosphate crystals, Cys, Asp, Asn, His, and standard ascorbic acid at different concentrations (50–1000 ppm).

H_2O_2 scavenging activities of all samples showed an increase from 50 ppm concentration to 1000 ppm. At all concentrations, the Hydrogen peroxide scavenging activity of ascorbic acid which was used as the positive control was the highest (97.01%, at 1000 ppm) among all samples. According to Table 1, H2O2 scavenging activities of amino acid-metal phosphate HNFs are higher than those of Cys, Asp, Asn, His, and metal phosphate crystals. Chemical formations on surfaces and the large surface area of Aa-metal phosphate HNFs were attributed to the decrease in H_2O_2 scavenging activities. Their results at 1000 ppm were as follows: Asn-Cu^{2+} HNFs, (48.03%), Asp-Cu^{2+} HNFs (59.84%), Cys-Cu^{2+} HNFs (54.20%), His-Cu^{2+} HNFs (64.00%), Asn-Co^{2+} HNFs (57.22%), Asp-Co^{2+} HNFs (52.15%), Cys-Co^{2+} HNFs (50.88%); His-Co^{2+} HNFs (44.62%), Asn-Zn^{2+} HNFs (39.65%), Asp-Zn^{2+} HNFs (42.4%), Cys-Zn^{2+} HNFs (40.04%) and His-Zn^{2+} HNFs (45.76%). H_2O_2 scavenging activities of AaHNFs varied depending on the metal in the structure: Aa-Cu^{2+} > Aa- Co^{2+} > Aa- Zn^{2+}. Hydrogen peroxide scavenging results of metal phosphate crystals at 1000 ppm were as follows: $Cu_3(PO_4)_2$ crystal (24.55%), $Co_3(PO_4)_2$ crystal (19.14%), and $Zn_3(PO_4)_2$ crystal (15.83%). The interaction with amino acids could have increased the hydrogen peroxide scavenging activity of those metal ions [47]. Hydrogen peroxide scavenging activity of amino acids was lower. Their results at 1000 ppm were as follows: Asp (17.50%), Asn (15.60%), His (14.91%), and Cys (10.09%). Their side chain negatively affected their hydrogen peroxide scavenging activity. According to Kim et al.; the thiol group in the Cys may serve as a substrate

Table 1 H_2O_2 scavenging activity (%) of AaHNFs at different concentrations

	% Scavenging activity				
	(1000 ppm)	(500 ppm)	(200 ppm)	(100 ppm)	(50 ppm)
Ascorbic acid	97.01 ± 0.0088	86.81 ± 0.0091	63.86 ± 0.0108	55.41 ± 0.0144	41.20 ± 0.0127
Asn-Cu^{2+}	48.03 ± 0.0117	27.94 ± 0.0105	17.25 ± 0.0122	9.40 ± 0.0095	4.94 ± 0.0071
Asp-Cu^{2+}	59.84 ± 0.0120	35.06 ± 0.0097	23.95 ± 0.0111	14.01 ± 0.0103	8.23 ± 0.0125
Cys-Cu^{2+}	54.20 ± 0.0093	32.08 ± 0.0115	21.93 ± 0.0111	12.43 ± 0.0130	7.63 ± 0.0125
His-Cu^{2+}	64.00 ± 0.0116	37.87 ± 0.0150	25.03 ± 0.0125	15.01 ± 0.0119	9.24 ± 0.0112
Asn-Co^{2+}	57.22 ± 0.0105	34.34 ± 0.0081	22.40 ± 0.0085	13.73 ± 0.0110	8.08 ± 0.0125
Asp-Co^{2+}	52.15 ± 0.0115	31.88 ± 0.0119	19.96 ± 0.0095	10.10 ± 0.0075	6.21 ± 0.0121
Cys-Co^{2+}	50.88 ± 0.0125	29.24 ± 0.0091	18.30 ± 0.0110	9.67 ± 0.0080	5.90 ± 0.0116
His-Co^{2+}	44.62 ± 0.0135	21.49 ± 0.0092	13.41 ± 0.0111	7.32 ± 0.0099	2.67 ± 0.0119
Asn-Zn^{2+}	39.65 ± 0.0101	16.73 ± 0.0095	7.50 ± 0.0085	3.16 ± 0.0107	–
Asp-Zn^{2+}	42.40 ± 0.0130	20.84 ± 0.0102	11.69 ± 0.0090	5.10 ± 0.0137	2.86 ± 0.0125
Cys-Zn^{2+}	40.04 ± 0.0110	17.01 ± 0.0106	9.14 ± 0.0111	4.21 ± 0.0102	1.40 ± 0.0111
His-Zn^{2+}	45.76 ± 0.0131	24.21 ± 0.0085	15.95 ± 0.0111	7.74 ± 0.0080	3.24 ± 0.0093
$Zn_3(PO_4)_2$ crystal	15.83 ± 0.0178	6.74 ± 0.0150	2.88 ± 0.0107	–	–
$Cu_3(PO_4)_2$ crystal	24.55 ± 0.0195	11.55 ± 0.0240	5.90 ± 0.0114	1.61 ± 0.0099	–
$Co_3(PO_4)_2$ crystal	19.14 ± 0.0160	9.05 ± 0.0142	4.47 ± 0.0133	–	–
Cys	10.09 ± 0.0131	5.57 ± 0.0145	3.16 ± 0.0091	1.79 ± 0.0110	–
Asp	17.50 ± 0.01122	9.68 ± 0.0138	6.87 ± 0.0118	3.34 ± 0.0106	–
His	14.91 ± 0.0131	8.79 ± 0.0132	5.98 ± 0.0119	2.49 ± 0.0090	–
Asn	15.6 ± 0.0105	9.28 ± 0.0085	5.12 ± 0.0090	1.68 ± 0.0101	–

for peroxidase in generating H_2O_2 [48]. H_2O_2 scavenging activity of cysteamine obtained by the degradation of cysteine was analyzed by Aruamo et al. They reported that the thiol group in structure negatively affected the H_2O_2 scavenging activity [49].

DPPH and ABTS radical scavenging activity of AaHNFs

Antioxidants play an important role against oxidative damage caused by free radicals and reactive oxygen species (ROS) which are thought to cause diseases. Various antioxidant defense mechanisms are available to counter the damage caused by ROS and free radicals. They reduce or eliminate the harmful effects of ROS or free radicals. Many methods are used to estimate antioxidant activities. DPPH and ABTS radical scavenging activities [2,2′-diphenylpicrylhydrazyl and 2,2′-azinobis (3-ethylbenzothiazoline-6-sulfonic acid) diammonium salt] are the most used ones among these methods due to their ease of measurement, short test time, and cheapness [50].

DPPH, firstly introduced by Blois in 1958 [42], and ABTS, developed by Re et al. [43], are methods in which color changes are used to determine free radical scavenging activity of Aa-metal phosphate HNFs. DPPH and ABTS scavenging activities of AaHNFs compared with the metal phosphate crystals, Cys, Asp, Asn, His, and

standard ascorbic acid at different concentrations (25–500 ppm) are shown, respectively, in Tables 2, 3. Decreases in the absorption of DPPH and ABTS radicals were monitored in all samples. Their DPPH and ABTS radical scavenging activities increased as the concentrations increased.

According to our assays, ascorbic acid which was used as the positive control displayed the most powerful DPPH radical scavenging activity at all concentrations among all of the samples. Cys, Asp, His, and Asn showed the strongest activity after ascorbic acid. For example, Ascorbic acid, Cys, Asp, His, and Asn exhibited 96.44%, 92.35%, 84.70%, 72.53%, and 66.55% at the same concentration (500 ppm), respectively. DPPH absorption of Aa-metal phosphate hybrid nanoflowers was higher than metal crystals but lower than amino acids. While the maximum DPPH radical scavenging activities of AaHNFs were calculated as 56.66% at 500 ppm, the maximum activities of metal crystals were calculated as 12.43%.

In comparison with all Aa-metal phosphate hybrid nanoflowers, it was highlighted by Guide et al. that some of the amino acids containing heteroatoms in their side chains such as Cys and Asp showed strong DPPH radical scavenging activities [51]. DPPH radical scavenging activity of AaHNFs was lower than amino acids due to the interaction of active side groups in amino acids with metal phosphate crystals during the formation of hybrid nanoflowers. Cys-Zn^{2+} hybrid nanoflowers exhibited the most powerful DPPH radical scavenging activities

Table 2 Effect of DPPH radical scavenging activity of AaHNFs at different concentrations

	% Scavenging activity				
	(500 ppm)	(250 ppm)	(100 ppm)	(50 ppm)	(25 ppm)
Ascorbic acid	96.44 ± 0.0091	85.00 ± 0.0112	4.,73 ± 0.0089	24.76 ± 0.0110	8.63 ± 0.0117
Asn-Cu^{2+}	28.19 ± 0.0081	16.57 ± 0.0075	6.32 ± 0.0110	3.09 ± 0.0122	–
Asp-Cu^{2+}	43.99 ± 0.0085	27.80 ± 0.0225	18.84 ± 0.0146	7.8 ± 0.0121	1.08 ± 0.0072
Cys-Cu^{2+}	49.66 ± 0.0136	33.89 ± 0.0104	19.74 ± 0.0125	11.59 ± 0.0106	2.92 ± 0.0087
His-Cu^{2+}	36.26 ± 0.0095	21.43 ± 0.0084	9.43 ± 0.0061	4.98 ± 0.0062	–
Asn-Co^{2+}	26.15 ± 0.0085	17.23 ± 0.0055	9.39 ± 0.0113	2.80 ± 0.0065	–
Asp-Co^{2+}	38.03 ± 0.0091	24.02 ± 0.0302	11.93 ± 0.0104	4.90 ± 0.0079	–
Cys-Co^{2+}	46.57 ± 0.0115	25.49 ± 0.0097	11.88 ± 0.0101	6.97 ± 0.0055	1.26 ± 0.0071
His-Co^{2+}	30.23 ± 0.0110	21.52 ± 0.0081	11.56 ± 0.0092	4.62 ± 0.0071	–
Asn-Zn^{2+}	32.49 ± 0.0102	17.95 ± 0.0050	9.4 ± 0.0072	7.11 ± 0.0110	–
Asp-Zn^{2+}	40.02 ± 0.0095	23.77 ± 0.0081	12.95 ± 0.0057	9.12 ± 0.0061	4.49 ± 0.0084
Cys-Zn^{2+}	56.66 ± 0.0117	39.86 ± 0.0076	17.46 ± 0.0107	9.51 ± 0.0086	3.80 ± 0.0082
His-Zn^{2+}	36.02 ± 0.0129	19.80 ± 0.0108	8.24 ± 0.0180	4.24 ± 0.0106	1.69 ± 0.0082
$Zn_3(PO_4)_2$ crystal	12.43 ± 0.0122	7.74 ± 0.0115	–	–	–
$Cu_3(PO_4)_2$ crystal	9.00 ± 0.0099	4.39 ± 0.0061	–	–	–
$Co_3(PO_4)_2$ crystal	8.97 ± 0.0117	3.91 ± 0.0091	–	–	–
Cys	92.35 ± 0.0073	66.90 ± 0.0085	34.66 ± 0.0076	21.62 ± 0.0082	6.39 ± 0.0095
Asp	84.70 ± 0.0091	61.71 ± 0.0082	31.48 ± 0.0095	16.22 ± 0.0117	470 ± 0.0102
His	72.53 ± 0.0087	43.47 ± 0.0106	25.38 ± 0.0114	11.71 ± 00,095	4.78 ± 0.0101
Asn	66.55 ± 0.0083	38.79 ± 0.0110	19.06 ± 0.0081	9.05 ± 0.007	3.43 ± 0.0102

Table 3 Effect of ABTS radical scavenging activity of AaHNFs at different concentrations

	% Scavenging activity (500 ppm)	% Scavenging activity (250 ppm)	% Scavenging activity (100 ppm)	% Scavenging activity (50 ppm)	% Scavenging activity (25 ppm)
Ascorbic acid	90.05 ± 0.0070	84.63 ± 0.0089	77.90 ± 0.0116	48.60 ± 0.0203	26.95 ± 0.0101
Asn-Cu^{2+}	38.63 ± 0.0105	22.63 ± 0.0091	14.14 ± 0.0115	9.31 ± 0.0152	5.65 ± 0.0091
Asp-Cu^{2+}	13.44 ± 0.0092	11.61 ± 0.0085	6.46 ± 0.0103	2.54 ± 0.0106	–
Cys-Cu^{2+}	71.20 ± 0.0100	42.12 ± 0.0131	25.31 ± 0.0086	16.00 ± 0.0102	10.29 ± 0.0097
His-Cu^{2+}	35.80 ± 0.0102	19.15 ± 0.0097	10.35 ± 0.0148	5.75 ± 0.0081	2.68 ± 0.0083
Asn-Co^{2+}	33.86 ± 0.0155	20.34 ± 0.0129	13.14 ± 0.0146	7.86 ± 0.0080	3.31 ± 0.0070
Asp-Co^{2+}	10.94 ± 0.0141	4.20 ± 0.0101	2.89 ± 0.0095	1.32 ± 0.0044	–
Cys-Co^{2+}	67.71 ± 0.0122	38.11 ± 0.0115	28.49 ± 0.0293	11.13 ± 0.0119	9.19 ± 0.0061
His-Co^{2+}	32.01 ± 0.0085	16.64 ± 0.0111	7.97 ± 0.0108	4.69 ± 0.0146	–
Asn-Zn^{2+}	30.17 ± 0.0105	19.47 ± 0.0080	12.86 ± 0.0106	6.53 ± 0.0098	3.77 ± 0.0092
Asp-Zn^{2+}	9.64 ± 0.0110	2.87 ± 0.0092	–	-	-
Cys-Zn^{2+}	61.69 ± 0.0092	35.52 ± 0.0081	23.13 ± 0.0120	10.86 ± 0.0100	5.61 ± 00,080
His-Zn^{2+}	29.09 ± 0.0090	14.11 ± 0.0091	8.37 ± 0.0107	3.83 ± 0.0080	–
$Zn_3(PO_4)_2$ crystal	14.99 ± 0.0179	8.01 ± 0.0121	2.26 ± 0.0090	-	–
$Cu_3(PO_4)_2$ crystal	23.28 ± 0.0083	10.02 ± 0.0101	4.67 ± 0.0118	–	–
$Co_3(PO_4)_2$ crystal	17.25 ± 0.0120	9.56 ± 0.0165	5.2 ± 0,0093	–	–
Cys	96.20 ± 0.0076	95.22 ± 0.0072	92.04 ± 0.0085	66.37 ± 0.0083	42.13 ± 0.0140
Asp	4.12 ± 0.0101	3.67 ± 0.0120	–	–	–
His	13.6 ± 0.0112	7.3 ± 0.0135	2.84 ± 0.0085	–	–
Asn	18.33 ± 0.0173	10.64 ± 0.0161	5.14 ± 0.0053	3.06 ± 0.0204	–

with 56.66%. DPPH radical scavenging activities of AaHNFs changed depending on the metal and amino acid in the structure. We evaluated the AaHNFs among themselves at the same concentration (500 ppm): The DPPH radical scavenging activities of Cys-Cu^{2+} HNFs, Asn-Cu^{2+} HNFs, Asp-Cu^{2+} HNFs, and His-Cu^{2+} HNFs were 49.66%, 28.19%, 43.99%, and 36.26%, respectively; the activities of Cys-Co^{2+} HNFs, Asn-Co^{2+} HNFs, Asp-Co^{2+} HNFs, and His-Co^{2+} HNFs were calculated to be 46.57%, 26.15%, 38.03%, and 30.23%, respectively; and the activities of Cys-Zn^{2+} HNFs, Asn-Zn^{2+} HNFs, Asp-Zn^{2+} HNFs, and His-Zn^{2+} HNFs were 56.66%, 32.49%, 40.02%, and 36.02%, respectively. DPPH radical scavenging activities of Cys-metal phosphate HNFs in the different amino acid-same metal groups exhibited the highest one. Cys-metal phosphate HNFs were followed by Asp-metal phosphate HNFs. These high activities depended on the structure of Cys and Asp. Some AaHNFs such as Asn-Zn^{2+} HNFs and Asn-Cu^{2+} HNFs showed no ABTS radical scavenging activity at some concentrations.

Cys and ascorbic acid inhibited ABTS free radicals at the rates of 96.20% and 90.05%, respectively, at 500 ppm (Table 3). Contrary to these results, inhibitions of ABTS free radicals by His, Asp, and Asn were very low being 13.60%, 4.12%, and 18.33% for each, respectively. DPPH radical scavenging activities of Asp, His, and Asn were higher than their ABTS radical scavenging activities. Generally, the ABTS radical scavenging activity of AaHNFs was more powerful than those of amino acids and metal crystals due to the interaction of active side groups in amino acids with metal phosphate crystals during the formation of hybrid nanoflowers. To compare the AaHNFs among themselves at 500 ppm; the activities of Cys-Cu^{2+} HNFs, Asn-Cu^{2+} HNFs, Asp-Cu^{2+} HNFs, and His-Cu^{2+} HNFs were 71.20%, 38.63%, 13.44% and 35.80%, respectively; the activities of Cys-Co^{2+} HNFs, Asn-Co^{2+} HNFs, Asp-Co^{2+} HNFs and His-Co^{2+} HNFs were 67.71%, 33.86%, 10.94% and 32.01%, respectively; and the activities of Cys-Zn^{2+} HNFs, Asn-Zn^{2+} HNFs, Asp-Zn^{2+} HNFs and His-Zn^{2+} HNFs were 61.69%, 30.17%, 9.64%, and 29.09%, respectively. Some Aa-metal phosphate HNFs such as Asp-Zn^{2+} HNFs and Asp-Cu^{2+} showed no ABTS radical scavenging activity at some concentrations. The phenolic group in His structure had limited ABTS radical scavenging activity because of the domination of hydrogen atom transfer.

Ascorbic acid is converted to ascorbate radical by giving an electron to lipid radical in order to finish the oxidative chain reaction. Ascorbate radicals react to form dehydroascorbate molecules that exhibit no antioxidant activity [52]. Due to the existence of thiol groups in its structure, a stronger antioxidant activity of Cys is observed. According to Guidea et al., amino acids like His or Asp which have amino [(–NH_2) or (–NH–)] or carboxyl (–COOH) groups in their side chains display powerful antioxidant behavior toward radicals because of their H^+ donating capability [51]. ABTS is based on electron transfer, while the DPPH method is based on H^+ transfer.

In summary, we developed the synthesis of AaHNFs considering Cu^{2+}, Mn^{2+}, Ni^{2+}, Co^{2+}, and Zn^{2+} metal ions and some amino acids which consist of imidazole ring, sulfhydryl group, carboxamide group, and acidic side chain (CH_2COOH). The characteristic properties of AaHNFs proved that amino acids are verified in the HNFs. AaHNFs exhibited a more effective peroxidase-like activity by using

Fenton's principle than free amino acids. In addition, AaHNFs can be evaluated as an effective anti-oxidant scavenger material due to their superior properties. Antioxidants play an important role in inhibiting the oxidative damage caused by free radicals and reactive oxygen species (ROS), which are thought to cause diseases. Various antioxidant defense mechanisms are available to counter the damage caused by ROS and free radicals. They reduce or eliminate the harmful effects of ROS or free radicals. The application of natural antioxidants is conventionally limited due to susceptibility to light, oxygen, and pH, poor solubility in physiological fluid, low bioavailability, and improper delivery in undesired cellular compartments. To overcome traditional problems, it is important to develop materials that form strong complexes with organic molecules and to determine their antioxidant capacity. Thus, it has been of our interest, to make and evaluate the synthesis of amino acid-metal phosphate hybrid nanoflowers which could serve as a potential application for procedures such as biosensing, bioassay, biomedicine, pharmaceutics, and biocatalysis to be able to personalize the biomaterials for a specific therapeutic agent and use these novel materials as drug carriers in different devices.

Supplementary Information The online version contains supplementary material available at https://doi.org/10.1007/s00289-021-03973-7.

Funding This work was financially supported by the Erciyes University Scientific Research Projects Unit (Grant number FBA-2017–7311).

Declarations

Conflict of interest The authors have no conflicts of interest to declare that are relevant to the content of this article.

References

1. Inupakutika MA, Sengupta S, Devireddy AR, Azad RK, Mittler R (2016) The evolution of reactive oxygen species metabolism. J Exp Bot 67(21):5933–5943. https://doi.org/10.1093/jxb/erw382
2. Koltover V (2018) Antioxidant biomedicine: from chemistry of free-radicals to reliability of biological systems. Rese Med Eng Sci. https://doi.org/10.31031/RMES.2018.03.000565
3. Ye F, Astete CE, Sabliov CM (2017) Entrapment and delivery of α-tocopherol by a self-assembled, alginate-conjugated prodrug nanostructure. Food Hydrocoll 72:62–72. https://doi.org/10.1016/j.foodhyd.2017.05.032
4. Souto EB, Severino P, Basso R, Santana MHA (2013) Encapsulation of antioxidants in gastrointestinal-resistant nanoparticulate carriers. Methods Mol Biol 1028:37–46. https://doi.org/10.1007/978-1-62703-475-3_3
5. Valgimigli L, Baschieri A, Amorati R (2018) Antioxidant activity of nanomaterials. J Mater Chem B 6(14):2036–2051. https://doi.org/10.1039/C8TB00107C
6. Ge J, Lei J, Zare RN (2012) Protein-Inorganic hybrid nanoflowers. Nat Nanotechnol 7(7):428–432. https://doi.org/10.1038/nnano.2012.80
7. Fang X, Zhang C, Qian X, Yu D (2018) Self-assembled 2,4-dichlorophenol hydroxylase-inorganic hybrid nanoflowers with enhanced activity and stability. RSC Adv 8(37):20976–20981. https://doi.org/10.1039/C8RA02360C
8. Yu J, Chen X, Jiang M, Wang A, Yang L, Pei X, Zhang P, Gang Wu, S. (2018) Efficient promiscuous knoevenagel condensation catalyzed by papain confined in Cu 3 (PO 4) 2 nanoflowers. RSC Adv 8(5):2357–2364. https://doi.org/10.1039/C7RA12940H

9. Altinkaynak C (2020) Hemoglobin-Metal2+ phosphate nanoflowers with enhanced peroxidase-like activities and their performance in visual detection of hydrogen peroxide. New J Chem. https://doi.org/10.1039/D0NJ04989A
10. Altinkaynak C, Tavlasoglu S, Kalin R, Sadeghian N, Ozdemir H, Ocsoy I, Özdemir N (2017) A hierarchical assembly of flower-like hybrid Turkish black radish peroxidase-Cu2+ nanobiocatalyst and its effective use in dye decolorization. Chemosphere 182:122–128. https://doi.org/10.1016/j.chemosphere.2017.05.012
11. Dayan S, Altinkaynak C, Kayaci Nilgün, Doğan ŞD, Özdemir N, KalayciogluOzpozan N (2020) Hybrid nanoflowers bearing tetraphenylporphyrin assembled on copper(II) or cobalt(II) inorganic material: A green efficient catalyst for hydrogenation of nitrobenzenes in water. Appl Organometal Chem. 34:e5381. https://doi.org/10.1002/aoc.5381
12. Zhu P, Wang Y, Li G, Liu K, Liu Y, He J, Lei J (2019) Preparation and application of a chemically modified laccase and copper phosphate hybrid flower-like biocatalyst. Biochem Eng J 144:235–243. https://doi.org/10.1016/j.bej.2019.01.020
13. Li Y, Wu H, Su Z (2020) Enzyme-based hybrid nanoflowers with high performances for biocatalytic, biomedical, and environmental applications. Coord Chem Rev 416:213342. https://doi.org/10.1016/j.ccr.2020.213342
14. Huang Y, Ran X, Lin Y, Ren J, Qu X (2015) Self-assembly of an organic-inorganic hybrid nanoflower as an efficient biomimetic catalyst for self-activated tandem reactions. Chem Commun (Camb) 51(21):4386–4389. https://doi.org/10.1039/c5cc00040h
15. Noma SAA, Yılmaz BS, Ulu A, Özdemir N, Ateş B (2020) Development of L-Asparaginase@ hybrid nanoflowers (ASNase@HNFs) reactor system with enhanced enzymatic reusability and stability. Catal Lett. https://doi.org/10.1007/s10562-020-03362-1
16. Baker YR, Chen J, Brown J, El-Sagheer AH, Wiseman P, Johnson E, Goddard P, Brown T (2018) Preparation and characterization of manganese, cobalt and zinc DNA nanoflowers with tuneable morphology, DNA content and size. Nucleic Acids Res 46(15):7495–7505. https://doi.org/10.1093/nar/gky630
17. Chaix A, Cueto-Diaz E, Delalande A, Knezevic N, Midoux P, Durand J-O, Pichon C, Cunin F (2019) Amino-acid functionalized porous silicon nanoparticles for the delivery of PDNA. RSC Adv 9(55):31895–31899. https://doi.org/10.1039/C9RA05461H
18. Park KS, Batule BS, Chung M, Kang KS, Park TJ, Kim MI, Park HG (2017) A simple and eco-friendly one-pot synthesis of nuclease-resistant DNA–inorganic hybrid nanoflowers. J Mater Chem B 5(12):2231–2234. https://doi.org/10.1039/C6TB03047E
19. Wei T, Du D, Zhu M-J, Lin Y, Dai Z (2016) An improved ultrasensitive enzyme-linked immunosorbent assay using hydrangea-like antibody-enzyme-inorganic three-in-one nanocomposites. ACS Appl Mater Interfaces 8(10):6329–6335. https://doi.org/10.1021/acsami.5b11834
20. Altinkaynak C, Baldemïr A, Özdemïr N, Yilmaz V, Öçsoy İ (2020) Kudret Narı (Momordica charantia Descourt) Meyvesinden Saflaştırılan Peroksidaz Enzimi Kullanılarak Hibrit Nano Çiçekler Sentezlenmesi ve Direct blue 1 Gideriminde Kullanılabilirlikleri. Bitlis Eren Üniversitesi Fen Bilimleri Dergisi 9(2):573–583. https://doi.org/10.17798/bitlisfen.603452
21 Altinkaynak C, Ildiz N, Baldemïr A, Özdemïr N, Yilmaz V, Öçsoy İ (2019) Synthesis of Organic-Inorganic Hybrid Nanoflowers Using Trigonella Foenum-Graecum Seed Extract and Investigation of Their Anti-Microbial Activity. Derim. https://doi.org/10.16882/derim.2019.549151
22. Wu Z-F, Wang Z, Zhang Y, Ma Y-L, He C-Y, Li H, Chen L, Huo Q-S, Wang L, Li Z-Q (2016) Amino acids-incorporated nanoflowers with an intrinsic peroxidase-like activity. Sci Rep. https://doi.org/10.1038/srep22412
23. Altinkaynak C, Gulmez C, Atakisi O, Özdemir N (2020) Evaluation of organic-inorganic hybrid nanoflower's enzymatic activity in the presence of different metal ions and organic solvents. Int J Biol Macromol 164:162–171. https://doi.org/10.1016/j.ijbiomac.2020.07.118
24. Shi Y, Liu L, Yu Y, Long Y, Zheng H (2018) Acidic amino acids: a new-type of enzyme mimics with application to biosensing and evaluating of antioxidant behaviour. Spectrochim Acta Part A Mol Biomol Spectrosc 201:367–375. https://doi.org/10.1016/j.saa.2018.05.024
25. Stone DL, Smith DK, Whitwood AC (2004) Copper amino-acid complexes–towards encapsulated metal centres. Polyhedron 23(10):1709–1717. https://doi.org/10.1016/j.poly.2004.04.001
26. Chandra A, Singh M (2018) Biosynthesis of amino acid functionalized silver nanoparticles for potential catalytic and oxygen sensing applications. Inorg Chem Front 5(1):233–257. https://doi.org/10.1039/C7QI00569E

27. Singh D, Singh SK, Atar N, Krishna V (2016) amino acid functionalized magnetic nanoparticles for removal of Ni(II) from aqueous solution. J Taiwan Inst Chem Eng 67:148–160. https://doi.org/10.1016/j.jtice.2016.06.017
28. Sun H, Zhao A, Gao N, Li K, Ren J, Qu X (2015) Deciphering a nanocarbon-based artificial peroxidase: chemical identification of the catalytically active and substrate-binding sites on graphene quantum dots. Angew Chem Int Ed 54(24):7176–7180. https://doi.org/10.1002/anie.201500626
29. Stanila A, Marcu A, Rusu D, Rusu M, David L (2007) Spectroscopic studies of some copper(II) complexes with amino acids. J Mol Struct 834–836:364–368. https://doi.org/10.1016/j.molstruc.2006.11.048
30. Gatlin CL, Turecek F, Vaisar T (2020) Copper(II) amino acid complexes in the gas phase https://pubs.acs.org/doi/pdf/https://doi.org/10.1021/ja00117a043 (accessed Dec 28, 2020). https://doi.org/10.1021/ja00117a043
31. Baran EJ, Viera I, Torre MH (2007) Vibrational Spectra of the Cu(II) Complexes of l-Asparagine and l-Glutamine. Spectrochim Acta Part A Mol Biomol Spectrosc 66(1):114–117. https://doi.org/10.1016/j.saa.2006.01.052
32. Aydemir D, Gecili F, Özdemir N, NurayUlusu N (2020) Synthesis and characterization of a triple enzyme-inorganic hybrid nanoflower (TrpE@ihNF) as a combination of three pancreatic digestive enzymes amylase, protease and lipase. J Biosci Bioeng 129(6):679–686. https://doi.org/10.1016/j.jbiosc.2020.01.008
33. Altinkaynak C, Kocazorbaz E, Özdemir N, Zihnioglu F (2018) Egg white hybrid nanoflower (EW-HNF) with biomimetic polyphenol oxidase reactivity: synthesis, characterization and potential use in decolorization of synthetic dyes. Int J Biol Macromol 109:205–211. https://doi.org/10.1016/j.ijbiomac.2017.12.072
34. Batule BS, Park KS, Gautam S, Cheon HJ, Kim MI, Park HG (2019) Intrinsic peroxidase-like activity of sonochemically synthesized protein copper nanoflowers and its application for the sensitive detection of glucose. Sens Actuators, B Chem 283:749–754. https://doi.org/10.1016/j.snb.2018.12.028
35. Shimazaki Y, Takani M, Yamauchi O (2009) Metal complexes of amino acids and amino acid side chain groups structures and properties. Dalton Trans 38:7854–7869. https://doi.org/10.1039/B905871K
36. Zhu J, Wen M, Wen W, Du D, Zhang X, Wang S, Lin Y (2018) Recent progress in biosensors based on organic-inorganic hybrid nanoflowers. Biosens Bioelectron 120:175–187. https://doi.org/10.1016/j.bios.2018.08.058
37. Sharma N, Parhizkar M, Cong W, Mateti S, Kirkland A, Puri M, Sutti A (2017) Metal ion type significantly affects the morphology but not the activity of lipase–metal–phosphate nanoflowers. RSC Adv 7(41):25437–25443. https://doi.org/10.1039/C7RA00302A
38. Lloyd RV, Hanna PM, Mason RP (1997) The origin of the hydroxyl radical oxygen in the fenton reaction. Free Radical Biol Med 22(5):885–888. https://doi.org/10.1016/S0891-5849(96)00432-7
39. Zhang B, Li P, Zhang H, Li X, Tian L, Wang H, Chen X, Ali N, Ali Z, Zhang Q (2016) Red-blood-cell-like BSA/Zn3(PO4)2 Hybrid particles: preparation and application to adsorption of heavy metal ions. Appl Surf Sci 366:328–338. https://doi.org/10.1016/j.apsusc.2016.01.074
40 Erdem HÜ, Kalın R, Özdemir N, Özdemir H (2015) Purification and biochemical characterization of peroxidase isolated from white cabbage (Brassica oleracea var capitata f. alba). Int J Food Properties 18:2099–2109. https://doi.org/10.1080/10942912.2014.963868
41. Ruch RJ, Cheng S-J, Klauning JE (1989) Prevention of cytotoxicity and inhibition of intercellular communication by antioxidant catechins isolated from chinese green tea. Carcinogenesis 10(6):1003–1008
42. Blois MS (1958) Antioxidant determinations by the use of a stable free radical. Nature 181(4617):1199–1200. https://doi.org/10.1038/1811199a0
43. Re R, Pellegrini N, Proteggente A, Pannala A, Yang M, Rice-Evans C (1999) Antioxidant activity applying an improved ABTS radical cation decolorization assay. Free Radical Biol Med 26(9):1231–1237. https://doi.org/10.1016/S0891-5849(98)00315-3
44. Zhuang J, Young AP, Tsung C-K (2017) Integration of biomolecules with metal-organic frameworks. Small 13(32):1700880. https://doi.org/10.1002/smll.201700880
45. Bryszewska M, Shcharbin D, Halets-Bui I, Abashkin V, Dzmitruk V, Loznikova S, Odabaşı M, Acet Ö, Önal B, Özdemir N, Shcharbina N (2019) Hybrid metal-organic nanoflowers and their application in biotechnology and medicine. Colloids Surf, B 182:110354. https://doi.org/10.1016/j.colsurfb.2019.110354

46. Hemnani T, Parihar M (1998) Reactive oxygen species and oxidative DNA damage. Indian J Physiol Pharmacol 42:440–452
47. Hertadi R, Amari MMS, Ratnaningsih E (2020) Enhancement of antioxidant activity of levan through the formation of nanoparticle systems with metal ions. Heliyon 6(6):e04111. https://doi.org/10.1016/j.heliyon.2020.e04111
48. Kim J-H, Jang H-J, Cho W-Y, Yeon S-J, Lee C-H (2020) In vitro antioxidant actions of sulfur-containing amino acids. Arab J Chem 13(1):1678–1684. https://doi.org/10.1016/j.arabjc.2017.12.036
49. Aruoma OI, Halliwell B, Hoey BM, Butler J (1988) The antioxidant action of taurine, hypotaurine and their metabolic precursors. Biochem J 256(1):251–255. https://doi.org/10.1042/bj2560251
50. Olszowy M, Dawidowicz AL (2018) Is it possible to use the DPPH and ABTS methods for reliable estimation of antioxidant power of colored compounds? Chem Pap 72(2):393–400. https://doi.org/10.1007/s11696-017-0288-3
51. Guidea A, Zăgrean-Tuza C, Moț AC, Sârbu C (2020) Comprehensive evaluation of radical scavenging, reducing power and chelating capacity of free proteinogenic amino acids using spectroscopic assays and multivariate exploratory techniques. Spectrochim Acta Part A Mol Biomol Spectrosc 233:118158. https://doi.org/10.1016/j.saa.2020.118158
52. Nimse SB, Pal D (2015) Free radicals, natural antioxidants, and their reaction mechanisms. RSC Adv 5(35):27986–28006. https://doi.org/10.1039/C4RA13315C